A New Hybrid Methodology According to NSM CFRP Technique for the Flexural Strengthening of RC Beams

Mohammadali Rezazadeh,[1] Joaquim Barros,[2]

ABSTRACT:

The objective of this paper is to propose a new hybrid methodology according to near surface mounted (NSM) technique, using carbon fiber reinforced polymer (CFRP) reinforcement for the flexural strengthening of reinforced concrete (RC) beams. This NSM hybrid flexural strengthening technique combines non-prestressed and prestressed CFRP laminates in the same application in order to provide a good balance in terms of load carrying and ultimate displacement capacity to the strengthened elements. An experimental program composed of six RC beams was carried out to assess the benefits of this NSM hybrid technique when compared to the use of non-prestressed or prestressed NSM CFRP laminates (NSM prestressing technique). For this purpose, the performance of both techniques in terms of crack width, prevailing failure mode, ultimate displacement capacity, energy absorption, and load carrying capacity of the strengthened beams was assessed. The experimental tests were also simulated by executing advanced 3D nonlinear finite element analysis. Moreover, the potentialities of other configurations for the NSM hybrid technique by adopting different non-prestressed CFRP reinforcement ratios were numerically assessed executing a parametric study, and the relevant results are presented and discussed.

Keywords: hybrid system, NSM technique, CFRP laminate, prestress force, flexural strengthening, numerical modeling.

[1] ISISE, PhD student of the Structural Division of the Dep. of Civil Engineering, University of Minho, 4800-058 Guimarães, Portugal. Rezazadeh.civil@gmail.com

[2] ISISE, Full Professor of the Structural Division of the Dep. of Civil Engineering, University of Minho, 4800-058 Guimarães, Portugal. Barros@civil.uminho.pt

1. Introduction

Extensive research has provided evidence for the efficiency of carbon fiber reinforced polymer (CFRP) composite materials for the flexural and shear strengthening of RC structures according to externally bonded reinforcing (EBR) or near surface mounted (NSM) techniques [1-6]. The NSM technique offers higher strengthening effectiveness than the EBR technique due to the higher confinement that the concrete surrounding the CFRP reinforcement provides to these composite materials [7].

The strengthening potentialities of high tensile strength of CFRP reinforcement can be mobilized by using composite material applied with a certain prestress level [8, 9]. The prestressed CFRPs provide an increase of load carrying capacity for deflection levels corresponding to the serviceability limit state (SLS) [10]. The maximum load capacity of the strengthened beams is, however, not influenced by the applied prestress level, while the load carrying capacity corresponding to concrete cracking and steel yield initiation has a tendency to increase with the prestress level [10]. Moreover, the prestressing system provides several additional strengthening benefits like closing the existing cracks, decreasing the crack width and cracked zone length, and reducing the probability of corrosion in steel reinforcement (durability benefit) [10, 11].

In spite of these benefits of prestressing system, the experimental results have indicated a decrease in terms of energy absorption and displacement ductility capacity up to failure of the strengthened beams, when the prestress level applied to the NSM CFRP reinforcement increases [8, 10, 12]. The energy absorption (E_d) is determined by integrating the area under the force-displacement curve up to the deflection at ultimate strength (δ_u), while the displacement ductility capacity is evaluated through a ductility index (μ_Δ) that is defined as ratio between the deflection corresponding to the ultimate strength (δ_u) and to the steel yield initiation (δ_y) of the beams ($\mu_\Delta = \delta_u/\delta_y$). This ductility criterion evaluates the ability of a structure to sustain plastic deformation without significant loss of load carrying capacity prior to collapse.

On the other hand, beams flexurally strengthened with FRP systems and applied according to EBR or NSM technique, do not present an almost perfectly plastic behavior after yielding of the longitudinal tensile steel bars, as is the case of

conventionally RC beams, since the FRP reinforcement has linear elastic behavior up to its brittle failure [13, 14]. Hence, in order to evaluate the ductility performance of FRP strengthened RC beams, deformability criterion was proposed by [15, 16] to evaluate the capacity of FRP strengthened beams to present, timely, signals of attaining collapse. Deformability index (μ_d) is defined as the ratio between the deflection corresponding to the failure (δ_u) and to the SLS conditions (δ_{SLS}) of the FRP strengthened beams ($\mu_d = \delta_u/\delta_{SLS}$).

The reduction of ultimate displacement capacity of the prestressed NSM CFRP beams with the increase of the prestress level is caused by the rupture of the CFRP reinforcement at smaller deflections, as a consequence of the initial tensile strain due to the prestress imposed to these composite materials. To improve the ultimate displacement capacity of NSM CFRP strengthened RC beams, partially bonded system (similar to fully bonded system except an unbonded portion of CFRP length at mid-span) was applied by [15]. Although the partially bonded strengthening has provided an improvement of the deformability compared to the fully bonded strengthening system, a slight decrease (4%-11%) was observed in terms of load carrying capacity at the steel yield initiation and at the failure when the corresponding values for the fully bonded system with similar prestress level were considered for comparison purpose.

Few studies have been dedicated to propose techniques for the enhancement of the ultimate displacement capacity of RC beams strengthened with prestressed NSM CFRP reinforcement (NSM prestressing technique). Hence, the purpose of the current study is to assess experimentally and numerically the potentialities of a new NSM hybrid strengthening methodology to enhance not only the load carrying capacity at SLS and ultimate conditions, but also the ultimate displacement and energy absorption capacity, when compared to the use of NSM prestressing technique. The proposed NSM hybrid technique combines non-prestressed and prestressed CFRP laminates in the same application for the flexural strengthening of RC beams. In this context an experimental program composed of RC beams strengthened according to the NSM prestressing and NSM hybrid techniques, using CFRP laminates, was carried out.

A 3D finite element (FE) model was adopted to simulate the experimental tests. This model is capable of simulating the nonlinear behavior of the constituent materials and the behavior of CFRP-adhesive-concrete interfaces, and the prestress process adopted in the test setup. After demonstrating the good predictive performance of this numerical

strategy, the efficiency of another configuration for the proposed NSM hybrid technique was numerically assessed for the flexural strengthening of RC beams, and the relevant results are presented and discussed.

2. Experimental Program

2.1. Beams and test setup

The experimental program was composed of six rectangular cross-section RC beams. One of the RC beams was kept un-strengthened as a control beam, while three RC beams were strengthened with a CFRP laminate prestressed at 0% (serving as a passive strengthened beam), 20%, and 40% of its nominal tensile strength, by adopting the NSM technique (designated as Pre-beams). The remaining two RC beams were strengthened by applying a NSM hybrid technique using non-prestressed and prestressed (20% and 40%) CFRP laminates in the same application (designated as HPre-beams).

Characteristics of the tested beams (geometry, loading configuration, support conditions and reinforcement details) are schematically represented in Figure 1 (dimensions are in mm). These simply supported beams were monotonically loaded up to failure under four-point loading configuration by imposing a displacement rate of 1.2 mm/min. The shear reinforcement ratio was designed to avoid shear failure for the RC beams ($\rho_{sw} = A_{sw}/b_w.s = 0.38\%$, where A_{sw} is the cross sectional area of a steel stirrup, b_w is the width of beam's cross section, and s is the spacing of the stirrups). The shear capacity of these beams, calculated according to the recommendations of [17] and [18], varies between 211 kN and 228 kN, which is slightly higher than the expected maximum flexural capacity for the strengthened beams ($\rho_s = A_s/b_w.d = 0.87\%$, where A_s is the cross sectional area of the tensile steel reinforcement, and d is its effective depth from top fiber of beam's cross section).

For the flexural strengthening of the RC beams according to the NSM prestressing technique, a CFRP laminate of 1.4 $\times$ 20 mm^2 cross sectional area was introduced into a groove (6×25 mm^2 cross section) pre-executed on the concrete tensile surface along the total beam length (sec.(A) in Figure 2). The CFRP laminate was bonded to the surrounding concrete with epoxy adhesive, and its extremities become at 50 mm before the supports (150 mm from the extremities of the beam) in order to simulate the anchorage conditions in a real applications (more details about the anchorage

conditions can be found elsewhere [10]). The tensile strains of the CFRP reinforcement in the passive strengthened beam were recorded by installing two strain gauges on the laminate (SG 1 and 2 shown in Figure 3), while for the prestressed strengthened beams, in addition of these two strain gauges, one more was installed on the prestressed laminate to better assess of the prestress losses (SG3 in Figure 3).

In the case of the hybrid strengthened beams, one additional passive CFRP laminate of 1.4×20 mm^2 cross sectional area was placed on each side of a prestressed CFRP laminate (1.4×20 mm^2 cross section) into the same groove (Figures 2 and 3) to provide an attempt of avoiding rupture of the prestressed CFRP laminate in the maximum bending moment region. At the location of the passive laminates, the groove size was increased to 15×25 mm^2 cross section (sec.(B) in Figure 2). The length of the passive laminates was extended at both extremities of the maximum bending moment region as development length represented in Figure 2. The development length was determined according to the recommendation of [1], $l_{db} \geq \left(a_b.b_b.f_{fd}\right)\big/\left(2.(a_b+b_b).\tau_b\right)$, where a_b and b_b are the thickness and height of the laminate's cross section, f_{fd} and τ_b are the tensile strength of CFRP and the average bond strength, respectively. By considering for a_b, b_b, f_{fd} and τ_b the values of 1.4 mm, 20 mm, 2000 MPa, and 6.9 MPa, respectively, it was obtained $l_{bd} \geq 190\,\text{mm}$, and a value of 300 mm was adopted due to the uncertainty in terms of the τ_b values. The tensile strain developed in the passive laminates was assessed by installing one strain gauge on the laminate (SG1 in Figure 3), while four strain gauges were installed on the prestressed laminate (SG 2, 3, 4 and 5 in Figure 3). To evaluate an eventual occurrence of a strain gradient in the prestressed laminate in the zone of the extremities of the passive laminates, SG 3 and 4 were installed at 50 mm before and after this section on the prestressed laminate, respectively. Moreover, one strain gauge was installed on the top fiber of the concrete at the mid-section of all the tested beams to monitor the concrete compressive strain ("Concrete SG" in Figure 3).

2.2. Prestressing system

The prestressing system represented in Figure 4 was designed to apply the prestress force to the CFRP reinforcement by taking advantage of an existing high stiff reaction steel frame in the laboratory of Minho University [19]. This prestress force was applied to the laminate at the sliding extremity of the prestressing system (Figure 4) using a hollow

hydraulic cylinder. This hydraulic cylinder was connected to a through-hole load cell to control release rate of the prestress force. Two steel rollers were placed under the beams to ensure a simultaneous release of the prestress force in both extremities of the RC beams. A more detailed description of the adopted prestressing system in the present experimental program (for laboratory conditions) can be found elsewhere [10], where the prestressing system for the flexural strengthening with NSM prestressed CFRP laminates on real conditions is also introduced. The applied prestress level was controlled by monitoring the average strain values of the strain gauges installed on the prestressed CFRP laminate (represented in Figure 3), considering the material properties reported by the manufacturer (elasticity modulus of 150 GPa and nominal tensile strength of 2000 MPa). The prestress force was totally removed after the recommended curing time for epoxy adhesive (72 hours at room temperature) adopting a relatively low releasing rate of 0.3 kN/min to avoid damage in the interface connections.

2.3. Material properties

The average values of the main properties for concrete, steel bars, CFRP laminate, and epoxy adhesive are indicated in Table 1, where the average compressive strength and Young's modulus of the concrete were evaluated from uniaxial compression tests on cylinders of 150 mm diameter and 300 mm height at the age of the beam tests (165 days).

3. Experimental Results

3.1. Load-displacement curves

The relationship between the applied load and the displacement at the mid-span for all the tested beams is depicted in Figure 5a. Regardless the prestress level, Figure 5a and Table 3 show an average increase of about 30% in terms of the maximum load carrying capacity for the beams strengthened with the NSM prestressing technique when compared to the control beam, while the average increase for the HPre-beams was about 44% when the same comparison is done. Figure 5b represents the strengthening efficiency in terms of load carrying capacity at concrete cracking, SLS conditions, steel yield initiation, and ultimate stage for all the strengthened beams, where the load capacities were normalized to the corresponding ones of the control beam. The SLS conditions for this experimental program were

adopted according to the requirements of the actual European design recommendations ($L/250 = 8.8 \, \text{mm}$, where L is the beam's span) [17].

Table 2 shows the main relevant results of the flexural response of the tested beams, where it can be confirmed that both strengthening techniques (Pre and HPre) have assured an increase in terms of load carrying capacity at concrete cracking (P_{cr}), SLS deflection conditions (P_{SLS}), and steel yield initiation (P_y), when the corresponding values of the passive strengthened beam are considered for comparison purposes, since an initial compression field in the tensile steel bars and surrounding concrete is introduced after the release of the prestress force. The increase of these force indicators is relatively small because only one prestressed laminate was applied in the Pre and HPre beams, which corresponds to a strengthening ratio of only 0.065%. However, the HPre-beams presented a higher increase in terms of the aforementioned force indicators and maximum load (P_u) without compromising the ultimate displacement capacity. This higher increase of the force indicators for the HPre-beams can be justified by the higher CFRP reinforcement ratio ($\rho_f = A_f/b_w.d_f = 0.195\%$, where A_f is the cross sectional area of the CFRP reinforcement, and d_f is its effective depth from top fiber of beam's cross section) in the maximum bending moment region.

As previously mentioned, all strengthened beams presented higher P_y than the control beam, which results in a higher safely margin at SLS conditions ($\left(P_y - P_{SLS}^{control}\right)/P_{SLS}^{control}$, where $P_{SLS}^{control}$ is the load corresponding to the SLS deflection of the control beam) based on the requirements of [17] (keeping the stress level in the longitudinal tensile steel bars below its yield strength) (Table 3). This increase of the safety margin was 13%, 19%, and 28% for the beams strengthened with the CFRP laminate prestressed at 0%, 20%, and 40% level, respectively, while the HPre-beams prestressed at 20% and 40% level presented an enhancement of 43% and 46% in terms of this safety margin, respectively. On the other hand, at the deflection limit corresponding to the SLS requirement, the NSM prestressing technique provided an increase of 4%, 6%, and 15% in terms of the load carrying capacity for prestress level of 0%, 20%, and 40%, respectively, when the control beam is considered for comparison purposes, while for the HPre-beams, the increase of the service load was 21% and 24%, for 20% and 40% prestress levels, respectively (Table 3).

According to Table 2, the energy absorption (E_d) and deformability (μ_d) indexes tended to decrease with the increase of the prestress force applied to the CFRP reinforcement. In fact, by increasing the prestress level in the laminate, the

rupture of the CFRP, when is the prevailing failure mode, occurs at a smaller deflection, resulting a decrease of the nonlinear response of the prestressed beams after steel yielding. Figure 6 shows the normalized indexes of energy absorption (E_d/E_d^{pas}) and deformability (μ_d/μ_d^{pas}) for the strengthened beams, where the E_d^{pas} and μ_d^{pas} are the energy absorption and deformability indexes of the passive strengthened beam.

Figure 6 evidenced that for 40% prestress level, the HPre-beam showed an enhancement of 24% and 9% in terms of energy absorption and deformability indexes, respectively, compared to the beam strengthened according to the NSM prestressing technique. For 20% prestress level, the HPre-beam developed an energy absorption similar to the beam strengthened with prestressed CFRP laminate (Pre-beam), while the NSM hybrid technique showed a decrease of 12% in terms of deformability index when compared to the use of NSM prestressing technique for the flexural strengthening of the beam. This fact can be justified by an unexpected premature failure of the 20% HPre-beam before the rupture of the prestressed laminate, which will be discussed in Section 3.3.

3.2. Internal strain distribution

At the maximum flexural capacity of the strengthened beams, the tensile strains recorded by the strain gauges installed on the laminates (see Figure 3) are depicted in Figure 7, where the prestrain value represents the initial tensile strain of the laminate after the release of the prestress force. Figure 7 evidences that the maximum tensile strain in the laminate of the beams strengthened with the NSM prestressing technique, has occurred in the maximum bending moment region, while in the case of the HPre-beams, due to the strengthening contribution of the passive laminates, the location of the maximum tensile strain in the prestressed laminate was transferred to just after the extremity of the passive laminates (SG4), which can postpone the failure of the prestressed laminate.

The relationship between the applied load and concrete compressive strain at the top fiber of the mid-section is represented in Figure 8 (data of the strain gauge in the control beam has not been reported due to the deficient functioning of this SG). This figure evidences that by increasing the level of the prestress force applied to the CFRP laminate, the Pre-beams exhibited a lower concrete compressive strain at the failure (as also observed by [10]). On the other side, the concrete compressive strains at the top fiber of the HPre-beams were, at the maximum beam's capacity, significantly lower than the compressive strains of the beams strengthened with the NSM prestressing

technique. This is justified by a downward of the position of the neutral axis, as well as a lower tensile strain in the laminates due to the higher flexural strengthening ratio in the region of highest bending moment in the HPre-beams.

3.3. Failure modes and crack patterns

The ultimate flexural capacity of all the tested beams was controlled by three types of failure modes after yielding of the tensile steel bars, namely: crushing of the concrete in the compression zone (CC); rupture of the laminate (CR); and concrete cover delamination (CD), as represented in Figure 9. In the control and passive strengthened beams, the concrete has crushed at the top zone of the central region of these beams (a maximum compressive strain of 0.0035 was recorded in the passive strengthened beam before the rupture of the laminate). In the passive strengthened beam, the laminate has ruptured immediately after concrete crushing. The beams strengthened with prestressed CFRP laminate failed by the rupture of the laminate due to the attainment of the ultimate tensile strength of the CFRP in a cracked section.

After yielding of the tensile steel bars, the HPre-beams experienced different failure modes, located at the end section of the passive laminates, as represented in Figure 9, while the failure modes of all other beams were located within the maximum bending moment region. Investigation of the crack widths in the HPre-beams evidenced that the cracks in the concrete surrounding the laminates in the region where the SG4 is located (Figures 3 and 9) were wider than the cracks at the SG3 section (Figures 3 and 9). This is supported by the higher tensile strain value recorded by the SG4 compared to the corresponding value of SG3 in the prestressed laminate of the HPre-beams, as shown in Figure 7. According to the principle of static equilibrium applied to the concrete placed between these two cracked sections, the shear (τ_s) and tensile (σ_t) stresses can be created in the weakest level along the concrete section (as shown in Figure 9). This weakest level is a plane just below the tensile steel bars due to a higher percentage of the voids formed during the concrete casting process (as previously confirmed by [20, 21]). At this weak plane's level, the tensile stress (normal to the plane), conjugated with the shear stress, can contribute to separate the concrete cover below the tensile steel bars by horizontally extending the cracks at the SG4 section. On the other side, the prestressed laminate (continuously passing from both SG3 and SG4 cracked sections) attempts to prevent this concrete cover separation.

During the bending loading process, by increasing the aforementioned stresses in the weak plane, the 20% HPre-beam showed a staircase pattern of load decay after the maximum flexural capacity (Figure 5a) due to the gradually separation of the concrete cover (cover delamination), while the 40% HPre-beam failed by rupturing of the prestressed CFRP laminate at a tensile strain less than its ultimate tensile strength (see Figures 7 and 9), since the weak plane's stresses may have contributed to the higher prestress level applied to the CFRP laminate. However, the 40% HPre-beam provided a higher maximum flexural capacity when compared to the corresponding value of the 20% HPre-beam (Table 2). In fact, by increasing the prestress level, a higher compressive strain field is created in the concrete cover below the tensile steel bars, which may provide more resistance in terms of opening and extending the cracks at the section of SG4, resulting in a higher flexural capacity for the strengthened beam when failing by concrete cover delamination.

The crack pattern of all the tested beams at the ultimate stage is shown in Figure 9, where most cracks consisted of flexural cracks. In the shear spans (defined between the point loading and the nearest support) flexural-shear cracks have formed. Due to the higher load carrying capacity of the HPre-beams, a more diffuse crack pattern with a predominance of shear cracks has formed in the shear spans of these beams, when compared to the other beams, since the shear capacity of all the beams is equal. Additionally, Figure 9 evidenced that by increasing the prestress level applied to the CFRP laminate, a decrease in terms of cracked zone length was observed in the Pre-beams due to an initial compressive strain field introduced by the prestress force. However, the HPre-beams showed longer cracked zone length compared to the Pre-beams due to a higher load carrying capacity provided by the hybrid strengthening system. The comparison between the cracked zone lengths for all the strengthened beams is indicated in Figure 10b, where the cracked zone lengths were normalized to the corresponding length of the control beam.

The relationship between the average crack width and applied load for the tested beams is represented in Figure 10a, where the average crack width was calculated by averaging the widths of the cracks located in the maximum bending moment region at the level of the tensile steel reinforcement. To evaluate the efficiency of the presented strengthening techniques in terms of limiting the crack width of the beams at SLS conditions, Figure 10b compares the average crack width of the strengthened beams at the SLS deflection limit (8.8 mm) normalized to the one registered in the control beam. Both prestressing and hybrid strengthening techniques showed a smaller average crack width when the prestress level applied to the CFRP laminate increases. This reduction of the average crack width was more noticeable in the

HPre-beams when compared to the Pre-beams with similar prestress level, which can be attributed to the higher flexural stiffness provided by the hybrid technique due to the contribution of the passive laminates.

4. Numerical Simulation

4.1. Description of finite element model

Previous research of the authors [10] evidenced that, a 3D finite element (FE) approach, capable of simulating the nonlinear behavior of the used materials, and the laminate-epoxy adhesive and concrete-epoxy adhesive interfaces, as well as, reproducing the real conditions for the experimental prestress process, can predict with high accuracy the behavior of RC beams strengthened with prestressed CFRP laminates applied according to the NSM technique. Hence, this numerical approach was used to simulate the experimental tests, by modeling one quarter of the beam, taking advantage of the double symmetry of the beams in order to reduce the computational time.

Figure 11 represents the finite element mesh of the hybrid strengthened beams, where a refined mesh was applied in the location where relatively high strain gradients are expected to develop. The support and loading conditions were simulated according to the characteristics of the test setup, and the experimental prestress process were reproduced adopting the real conditions in laboratory (1st applying the prestress force; 2nd introducing the interfaces; 3rd release the prestress force at both extremities of the CFRP reinforcement).

Eight-node solid elements were used for the concrete, and the Concrete Damaged Plasticity (CDP) model was adopted to simulate the concrete's nonlinear behavior. The CDP model considers two main damage mechanisms of the concrete, namely, cracking formation and propagation in tension, and elasto-plasticity in compression [22]. The uniaxial behavior of the uncracked concrete in tension and compression was assumed to be linear up to f_t (concrete tensile strength: 1.8 MPa) and $0.45 f_c'$ (concrete compressive strength: 24.5 MPa), respectively, while stress-crack opening and stress-strain relations for uniaxial tension and compression of the cracked concrete were obtained according to the recommendation of CEB-FIP model code (with tensile fracture energy, G_f, of 0.07 N/mm) (Figure 12a and 12b) [18, 23].

The constitutive parameters of the CDP model (dilation angle ϕ, plastic potential eccentricity e, stress ratio f_{b0}/f_{c0}, shape of the loading surface K_c, viscosity parameter V) were estimated based on the recommended range of values by [22, 24], and are included in Figure 12a. The parameters ϕ and e represent the shape of the flow potential function that were determined based on the proposed ranges for ϕ (34° - 43°) and e (1 – 1.5) [24], while f_{b0}/f_{c0} and K_c describe the shape of the yield function, and the adopted values are the default ones recommended by CDP model [22]. The value of V parameter was assumed to be zero in this analysis.

Steel reinforcement was perfectly bonded to the concrete by embedding 3D two-node truss elements into the concrete elements. An idealized elasto-plastic model with associated plastic flow was assigned to these truss elements to simulate the behavior of the steel bars up to its ultimate tensile strength based on the simplified model recommended by CEB-FIP code [23] ($f_{sy} = 563\,\text{MPa}$ and $f_{su} = 656\,\text{MPa}$ represented in Figure 12c). Eight-node solid elements were adopted to model the CFRP laminate and epoxy adhesive. A perfect plasticity model, with no hardening, was used to simulate the epoxy adhesive behavior represented in Figure 12c ($f_e = 20\,\text{MPa}$), while the tensile behavior of the CFRP laminates was assumed to be linear up to its ultimate tensile strength ($f_f = 1922\,\text{MPa}$, represented in Figure 12d). After ultimate tensile strain, ε_{fu}, the contribution of the laminates is neglected.

To consider debonding aspects in the FE model, two surface-based contact interfaces between concrete-epoxy adhesive and laminate-epoxy adhesive were defined. A mixed mode of normal stress-separation and shear stress-slip was used to model concrete-epoxy interface, while shear stress-slip mode was only considered to simulate the behavior of the laminate-epoxy interface. Damage evaluation of the interfaces was defined by a linear softening branch considering the fracture energy of the interfaces (Figures 12e and 12f).

The normal tensile stress and tensile fracture energy of the concrete-epoxy interface was limited to the tensile strength and fracture energy of the concrete ($\sigma_{n,max} = f_t = 1.8\,\text{MPa}$, $G_{n,f} = G_f = 0.07\,\text{N/mm}$), while the maximum shear stress and shear fracture energy of this bond was obtained from the model recommended by [25] ($\tau_{s,max} = 7.1\,\text{MPa}$, $G_{s,f} = 6.4\,\text{N/mm}$). The maximum shear stress of the laminate-epoxy interface was found from the literature [26] (

$\tau_{s,max} = 20\,\text{MPa}$), while the shear fracture energy corresponding to this interface was estimated by calculating the area under the proposed shear stress-slip curve [26] ($G_{s,f} = 23.56\,\text{N/mm}$).

4.2. Assessment of the numerical strategy

The predictive performance of the described numerical model was assessed by simulating all the tested beams, and the comparison of the applied load *versus* mid-span displacement response obtained numerically and experimentally is depicted in Figure 13. This figure indicates a good predictive performance of the numerical strategy in terms of the flexural response of the tested beams. Moreover, in the cases of the control beam and beams strengthened with prestressed laminate at 0%, 20%, and 40% level, the numerical model predicted with good accuracy the displacement level when the concrete crushing and the rupture of the CFRP have occurred experimentally.

For the flexural response of the hybrid strengthened beams, the numerical model estimates an almost constant load carrying capacity after the development of high stress gradient in the zone where experimentally an intense damage evolution was observed (Figure 9). The instant of the development of this stress gradient higher than the concrete tensile resistance was pointed on the numerical flexural response of the HPre-beams in Figure 13, as a stage when the concrete cover below the tensile steel bars cannot sustain the created stress concentration, and concrete cover delamination can occur. Finally, the failure modes registered experimentally were captured numerically, but for displacement levels higher than the ones observed experimentally. This fact can be attributed to the use of embedded truss elements within the concrete elements to model the longitudinal tensile steel bars, preventing to create the weak plane just below the tensile steel bars in the concrete. The concrete tensile strain field based on the PEEQT output (equivalent plastic strain in uniaxial tension) of the FE software is represented in Figure 14 for the prestressed and hybrid strengthened beams at the maximum capacity [22].

5. Evaluation of another configuration of the NSM hybrid technique

This section aims to numerically evaluate the efficiency of passive CFRP reinforcement ratio of the NSM hybrid technique (lower than the one adopted in the experimental program), on the prevailing failure mode and ultimate

displacement capacity of the strengthened beams. For this purpose, another configuration for combining passive and prestressed CFRP laminates based on the NSM hybrid technique was adopted for the flexural strengthening of the RC beams. This configuration was composed of two prestressed CFRP laminates of 1.4×10 mm^2 cross sectional area and one passive CFRP laminate of either 1.4×10 mm^2 (designated as HPre-L10, sec. (A1) in Figure 15) or 1.4×20 mm^2 (designated as HPre-L20, sec. (A2) in Figure 15) cross sectional area, introduced in separate grooves. The ratio of the prestressed CFRP reinforcement of this configuration was adopted similar to the corresponding ones in the experimental program ($\rho_{f(pre)} = 0.065\%$), and was also prestressed at 20% and 40% of its nominal tensile strength (Figure 15). The total length of the passive laminates was determined for fulfilling the development length adopted in the experimental tests (Figure 2).

The RC beams strengthened with the proposed hybrid configuration (represented in Figure 15) were simulated using the described FE model, and the applied load *versus* mid-span displacement responses are represented in Figure 16a and 16b for 20% and 40% prestress levels, respectively. This figure also numerically compares the flexural response of HPre-L10 and HPre-L20 beams with the Pre and HPre beams adopted in the experimental tests (designated as Pre-FE and HPre-FE, respectively) with similar prestress level.

Figures 16a and 16b evidence that, regardless the prestress level, both HPre-L10 beams (prestressed at 20% and 40% level) failed by yielding of the tensile steel bars followed by the rupture of the prestressed CFRP laminates due to the attainment of its ultimate tensile strength at the end section of the passive laminate, while the HPre-L20 beams prestressed at 20% and 40% level experienced different failure modes after yielding of the tensile steel bars at the end section of the passive laminate. For 20% prestress level, the HPre-L20 beam failed by concrete cover delamination, while rupture of the prestressed laminates occurred in the 40% HPre-L20 beam. In fact, as previously mentioned (section 3.3), by increasing the prestress level, due to the higher compressive strain field in the concrete cover below the tensile steel bars, a higher resistance to the susceptibility of concrete cover delamination can be provided for the hybrid strengthened beams. This higher resistance when conjugated with the higher initial tensile strain introduced in the CFRP, can result to increase the possibility of occurrence of the rupture of the prestressed laminates before the concrete cover delamination.

Table 4 presents the most relevant results of the flexural response of the beams simulated in this section. It can be confirmed that, regardless the prestress level, by increasing the passive CFRP reinforcement ratio ($\rho_{f(pas)}$) of the hybrid beams, the load carrying capacity corresponding to the steel yield initiation stage has increased, as well as the corresponding deflection. On the other hand, increasing the passive CFRP reinforcement ratio has provided a higher ultimate displacement capacity and energy absorption index when the hybrid beams have failed by rupture of the prestressed laminates. In fact, the ultimate displacement capacity of the hybrid beams can significantly be affected by the prevailing failure mode at this stage.

Figures 16c and 16d show the normalized indexes of energy absorption (E_d/E_d^{pas}) and deformability (μ_d/μ_d^{pas}) for the simulated beams prestressed at 20% and 40% level, respectively, where the (E_d^{pas}) and (μ_d^{pas}) are the energy absorption and deformability indexes of the numerical response of the passive strengthened beam. This figure shows that, for 20% prestress level, the HPre-L10 beam (with $\rho_{f(pas)} = 0.032\%$) presented the highest energy absorption and deformability indexes amongst the beams strengthened according to the NSM hybrid technique, while for 40% prestress level, the HPre-L20 beam (with $\rho_{f(pas)} = 0.065\%$) provided the highest values for these indexes. Hence, it can be concluded that, regardless the prestress level, the increase of the passive CFRP reinforcement ratio ($\rho_{f(pas)}$) of the hybrid strengthened beams provides a higher energy absorption and deformability indexes when the rupture of the prestressed laminates (located at the end section of the passive laminate) is observed at the maximum capacity as governing failure mode.

6. Conclusion

This work aimed to explore a new hybrid methodology according to the near surface mounted (NSM) technique, using the carbon fiber reinforced polymer (CFRP) reinforcement for the flexural strengthening of reinforced concrete (RC) beams. This NSM hybrid technique combines non-prestressed and prestressed CFRP laminates in the same application. The efficiency of the proposed NSM hybrid technique for the flexural strengthening was evaluated by performing an experimental program composed of six RC beams. The experimental tests were simulated by a 3D nonlinear finite element model and then, the potentialities of other configurations for the NSM hybrid technique were

numerically assessed. According to the obtained results from the current study, the following conclusions can be drawn:

- NSM hybrid strengthening technique provided a higher strengthening efficiency in terms of load carrying capacity at concrete cracking, SLS conditions and steel yield initiation, when compared to the use of NSM prestressing technique for the flexural strengthening of RC beams.

- The hybrid strengthened beams provided an average increase in terms of ultimate load carrying capacity higher than the ones obtained for the prestressed strengthened beams, when compared to the results obtained for the control beam. This ultimate flexural capacity of the hybrid beams was influenced by the prestress level applied to the CFRP laminate, due to the different prevailing failure modes.

- The ultimate flexural capacity of all the tested beams was controlled by three types of failure modes after yielding of the tensile steel bars, namely: crushing of the concrete (CC); rupture of the CFRP laminate (CR); and concrete cover delamination (CD). The failure modes of the control and prestressed strengthened beams (CC and CR) were located within the maximum bending moment region, while the hybrid strengthened beams failed (by CR and CD) at the end section of the passive laminates. Moreover, the results showed that both prestressing and hybrid techniques decrease the possibility of the CC as prevailing failure mode of the strengthened beams, while this reduction was more evident when hybrid technique was adopted for strengthening application.

- Both prestressing and hybrid strengthening techniques showed a smaller average crack width when the prestress level applied to the CFRP laminate increases. This reduction of the average crack width was more noticeable in the hybrid beams when compared to the prestressed beams with similar prestress level.

- Reduction of the ultimate displacement capacity of the prestressed NSM CFRP beams was observed with the increase of the prestress level, resulting a decrease in terms of energy absorption and deformability indexes, while the aforementioned indicators for the hybrid NSM CFRP beams were influenced by the type of prevailing failure mode at the maximum capacity (CR or CD). The hybrid strengthened beam, failed by the CR failure mode at the maximum capacity, showed a higher energy absorption and deformability indexes compared to the prestressed strengthened beam with similar prestress level.

- A 3D finite element (FE) model was adopted to simulate the experimental tests, and its good predictive performance was demonstrated. This model is capable of simulating the nonlinear behavior of the constituent materials, CFRP-adhesive-concrete interfaces, and the prestress process adopted in the test setup.

- The efficiency of another configuration for the proposed NSM hybrid technique was numerically assessed for the flexural strengthening of RC beams. The results of this numerical analysis showed that, by increasing the passive CFRP reinforcement ratio in the hybrid system, a higher energy absorption and deformability indexes, when the CR failure occurs before the CD failure at the maximum capacity, can be achieved for the hybrid strengthened beams. The highest energy absorption and deformability indexes for the simulated hybrid beams were numerically obtained with an average increase of 21% and 37%, respectively, when the corresponding values of the prestressed NSM CFRP beam with similar prestress level are considered for comparison purpose.

7. Acknowledgments

8. Reference

[1] ACI-440.2R. Guide for the Design and Construction of Externally Bonded FRP Systems for Strengthening Concrete Structures. *American Concrete Institute*, 2008.

[2] Barros J and Fortes A. Flexural Strengthening of Concrete Beams with CFRP Laminates Bonded into Slits. *Cement and Concrete Composites*. 2005;27(4) p:471-80.

[3] Nanni A. North American Design Guidelines for Concrete Reinforcement and Strengthening using FRP: Principles, Applications and Unresolved Issues. *Construction and Building Materials*. 2003;17:439–46.

[4] Dias S and Barros J. Shear Strengthening of RC Beams with NSM CFRP Laminates: Experimental Research and Analytical Formulation. *Composite Structures*. 2012;99:477-90.

[5] Dias S and Barros J. Shear Strengthening of RC T-section Beams with Low Strength Concrete Using NSM CFRP Laminates. *Cement & Concrete Composites*, 2010.

[6] Jayaprakash J, Pournasiri E, Choong K, Tan C and De'nan F. External CFRP Repairing of Pretested Beams Reinforced Using Prestress Rebars. *Reinforced Plastics and Composites*, 2011;30(20):1753-68.

[7] Barros J, Dias S and Lima J. Efficacy of CFRP-based Techniques for the Flexural and Shear Strengthening of Concrete Beams. *Cement and Concrete Composites*, 2007;29(3).

[8] Nordin H and Taljsten B. Concrete Beams Strengthened with Prestressed Near Surface Mounted CFRP. *Journal of Composites for Construction*, 2006;10(1):60-8.

[9] Badawi M and Soudki K. Flexural Strengthening of RC Beams with Prestressed NSM CFRP Rods- Experimental and Analytical Investigation. *Construction and Building Materials*. 2009:3292-300.

[10] Rezazadeh M, Costa I and Barros J. Influence of Prestress Level on NSM CFRP Laminates for the Flexural Strengthening of RC Beams. *Composite Structures*. 2014;116:489-500.

[11] Hajihashemi A, Mostofinejad D and Azhari M. Investigation of RC Beams Strengthened with Prestressed NSM CFRP Laminates. *Journal of Composites for Construction (ASCE)*. 2011;15(6.).

[12] Rezazadeh M, Costa I and Barros J. Assessment of the Effectiveness of Prestressed NSM CFRP Laminates for the Flexural Strengthening of RC Beams. In: Proceedings of *FRPRCS11*. Guimaraes, Portugal., Conference, 2013.

[13] Jo B, Tae G and Kwon B. Ductility Evaluation of Prestressed Concrete Beams with CFRP Tendons. *Reinforced Plastics and Composites*. 2004;23:834.

[14] Oudah F and El-Hacha R. A New Ductility Model of Reinforced Concrete Beams Strengthened Using Fiber Reinforced Polymer Reinforcement. *Composites: Part B*; 2012 43:3338-47.

[15] Choi H, West J and Soudki K. Effect of Partial Unbonding on Prestressed Near-Surface-Mounted CFRP-Strengthened Concrete T-Beams. *Journal of Composites for construction (ASCE)*. 2011;15(1.).

[16] Choi H, Flexural Behaviour of Partially Bonded CFRP Strengthened Concrete T-Beams, *PhD thesis*, University of waterloo, Canada, 2008.

[17] EN 1992-1-1. Design of Concrete Structures. Part 1-1: General Rules and Rules for Buildings. 2004.

[18] ACI 318-05. Building Code Requirements for Structural Concrete.: *ACI Committee 318.*; 2005.

[19] Costa I and Barros J. Design and Development of Hydraulic-Electro-Mechanical System to Apply Pre-Stressed CFRP Laminates According to the NSM Technique in Laboratory Conditions. *Technical Report No. 12-DEC/E-12, University of Minho*; 2012. p. 59.

[20] Xiong G, Jiang X, Liu J and Chen L. A Way for Preventing Tension Delamination of Concrete Cover in Midspan of FRP Strengthened Beams. *Construction and Building Materials*. 2007;21:402–8.

[21] Barros J, Costa I and Gouveia A. CFRP Flexural and Shear Strengthening Technique for RC Beams: Experimental and Numerical Research. *Advance in Structural Engineering*. 2011;14(3.).

[22] ABAQUS. Abaqus Analysis User's Manual. 2011.

[23] CEB-FIP. Model Code 2010. Final draft *fib, CEB-FIP*.; 2011.

[24] Jankowiak T and Lodigowski T. Identification of Parameters of Concrete Damage Plasticity Constitutive Model. *Foundation of civil and environmental engineering*. 2005(6.).

[25] Seracino R, Saifulnaz M and Oehlers D. Generic Debonding Resistance of EB and NSM Plate-to-Concrete Joints. *Journal of Composites for construction (ASCE)*. 2007;11(1.).

[26] Cruz J and Barros J. Modeling of Bond between Near Surface Mounted CFRP Laminate Strips and Concrete. *Computers and Structures*. 2004:1513-21.
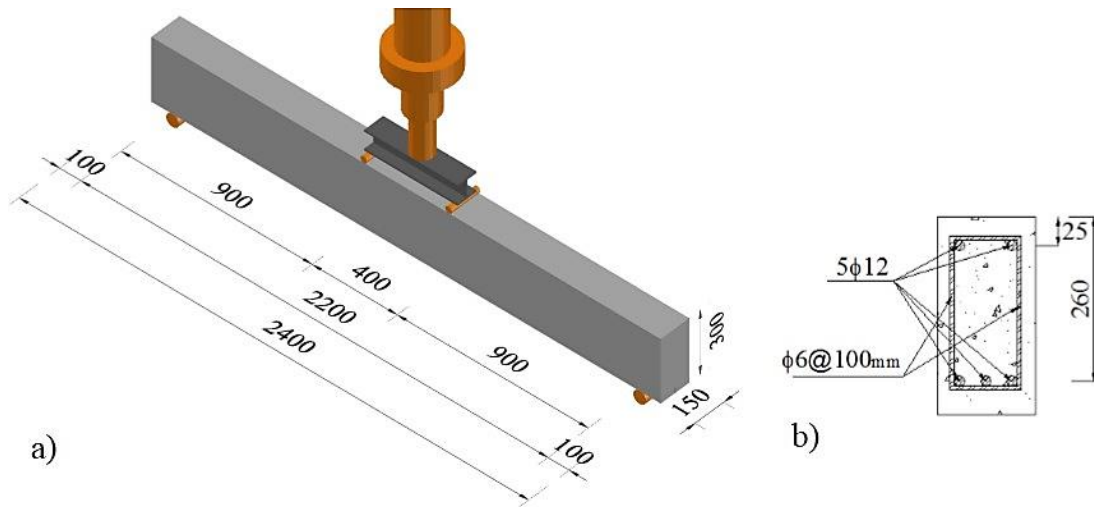
Figure 1: The beams of the experimental program: a) geometry and loading configuration; b) steel reinforcement (dimensions in mm)
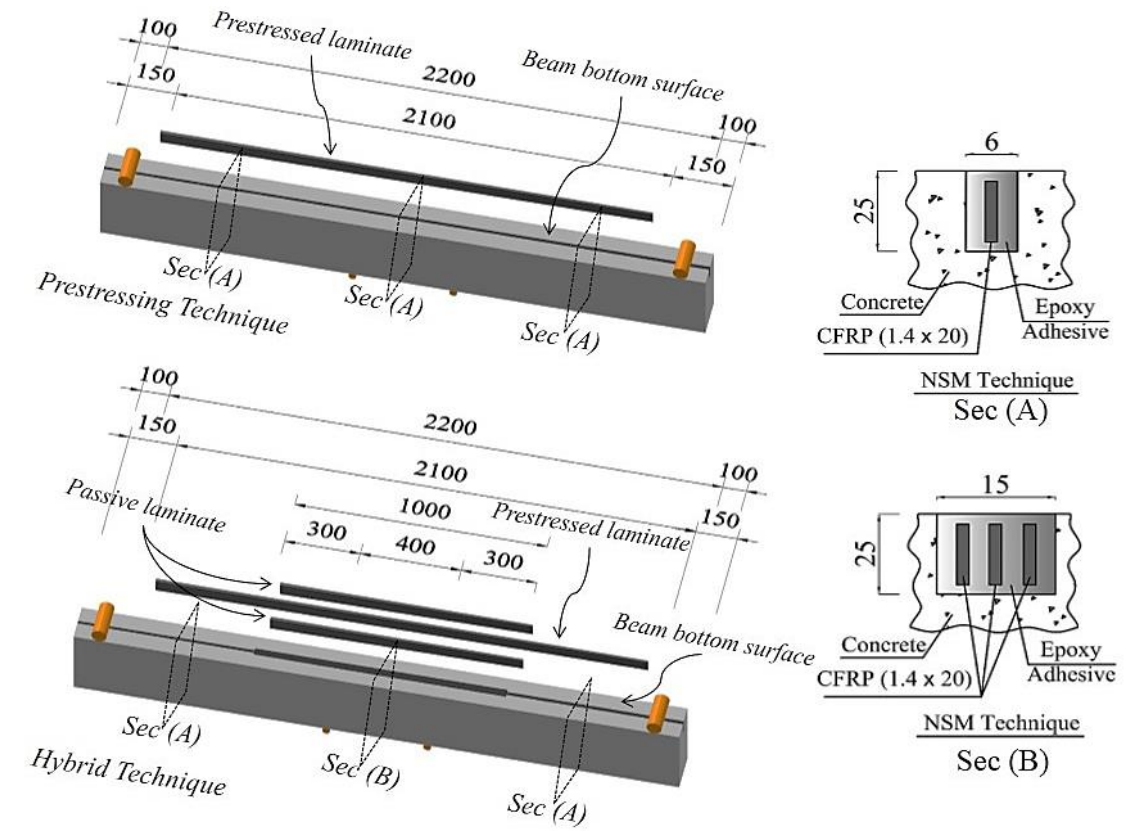
Figure 2: CFRP reinforcement details of hybrid and prestressing NSM techniques (dimensions in mm) (the beams are intentionally represented upside down to reveal the grooves)
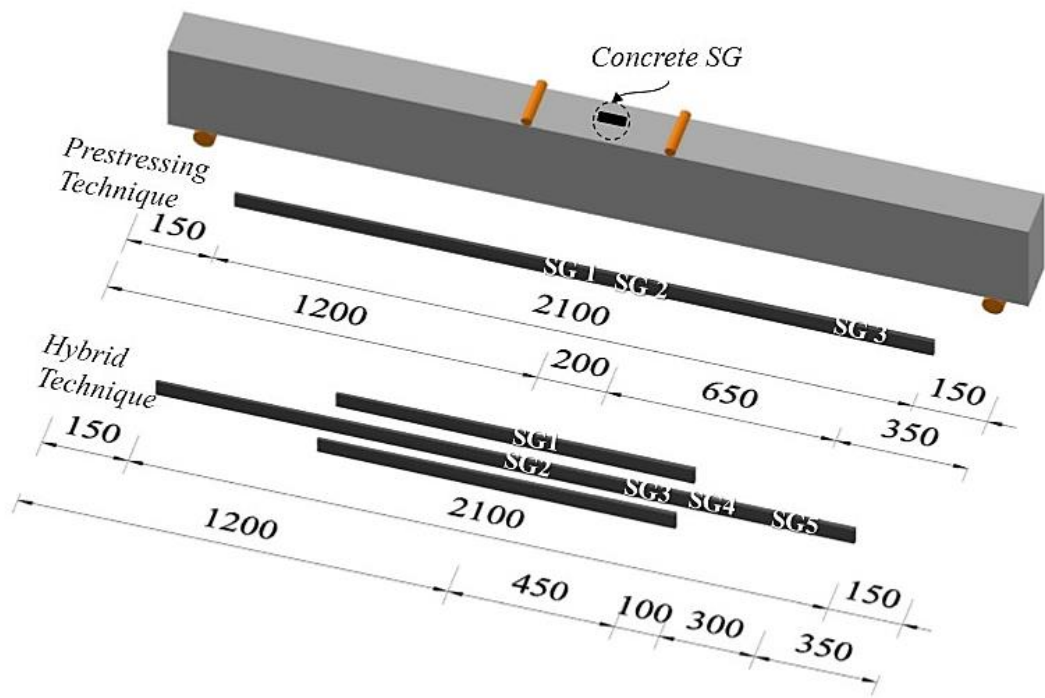
Figure 3: Position of the strain gauges (SG) installed on the CFRP laminates and concrete (dimensions in mm)
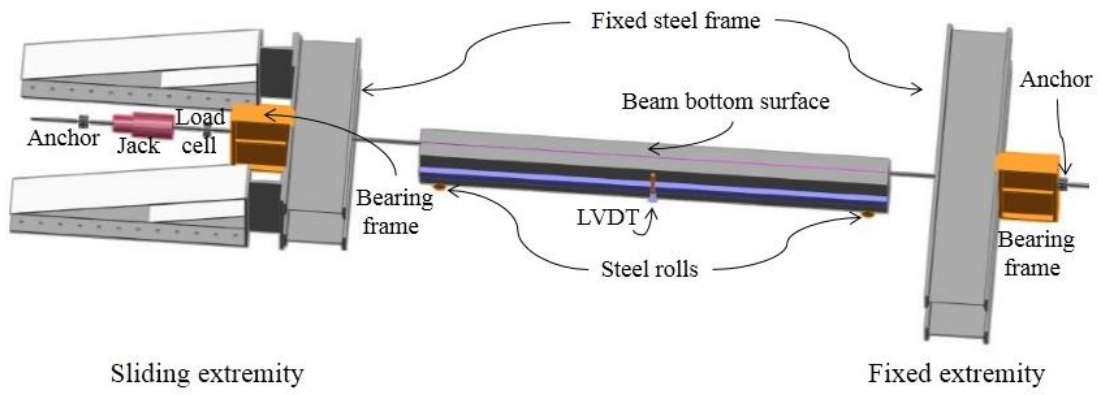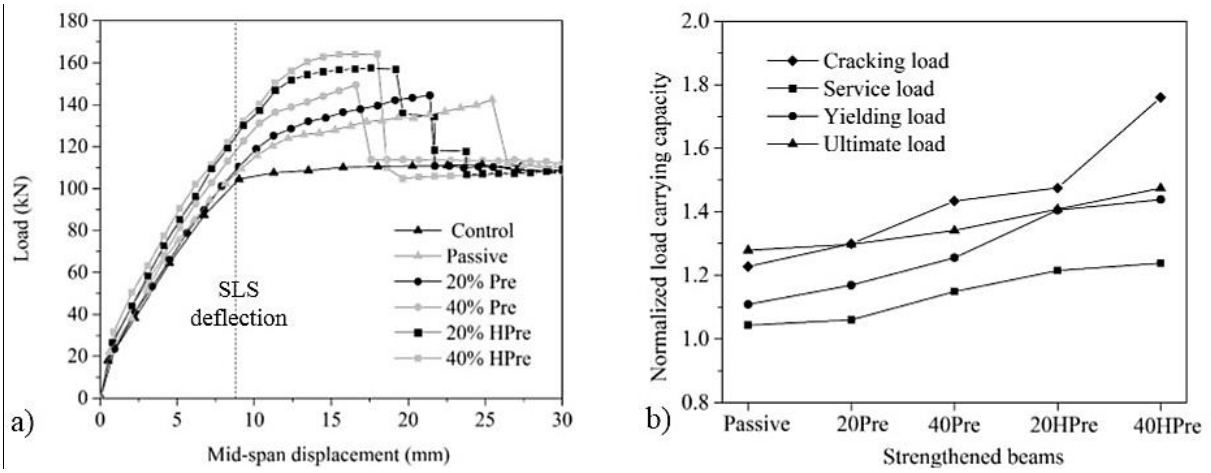
Figure 4: Prestressing system

Figure 5: a) Load *versus* mid-span displacement of the tested beams, b) load capacities at concrete cracking, SLS deflection, steel yielding, and ultimate point normalized to the control beam
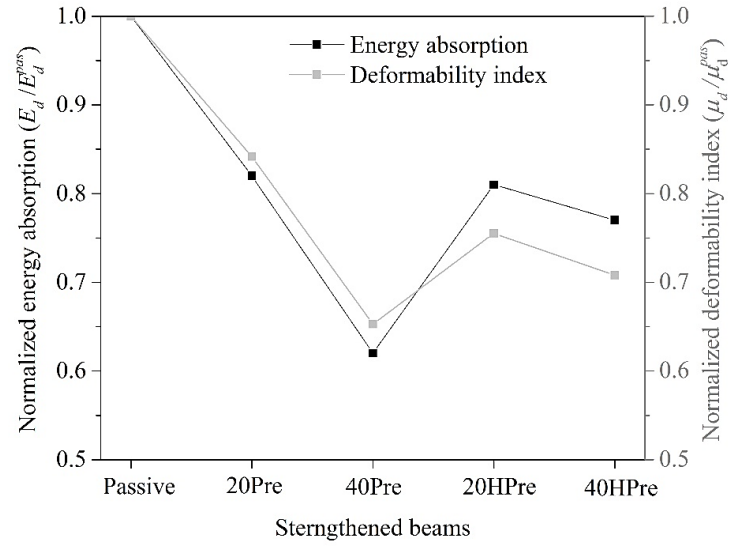
Figure 6: Energy absorption and deformability indexes normalized to the passive strengthened beam
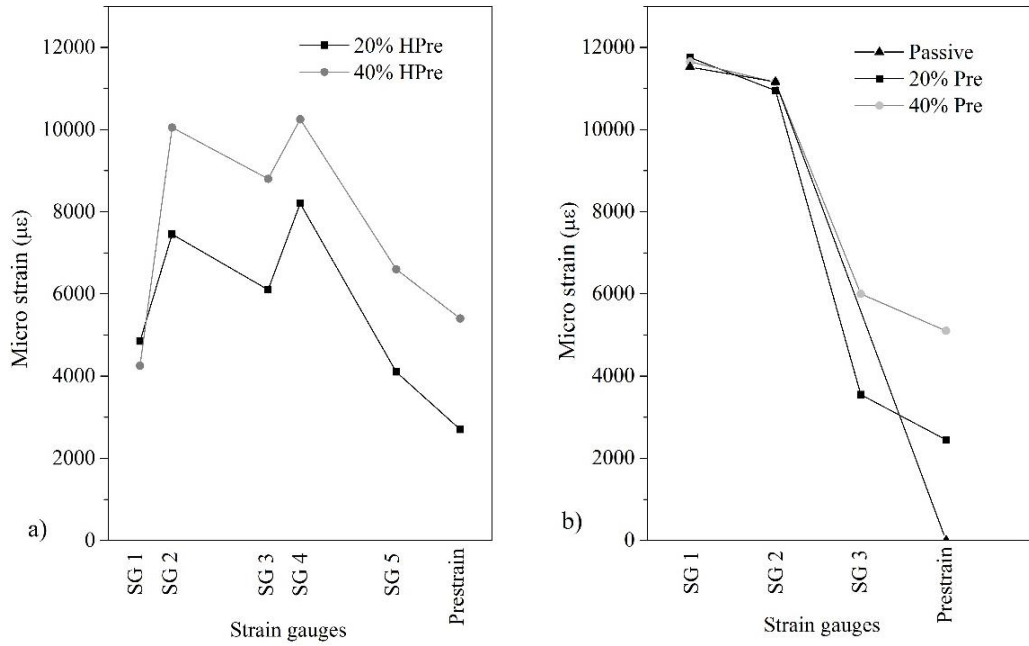
Figure 7: Tensile strains of the CFRP laminate at maximum load: a) hybrid strengthened beams; b) beams strengthened with NSM prestressing technique
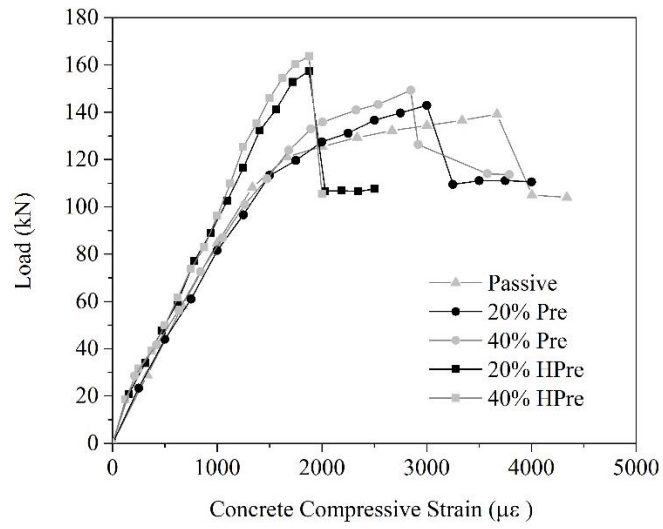
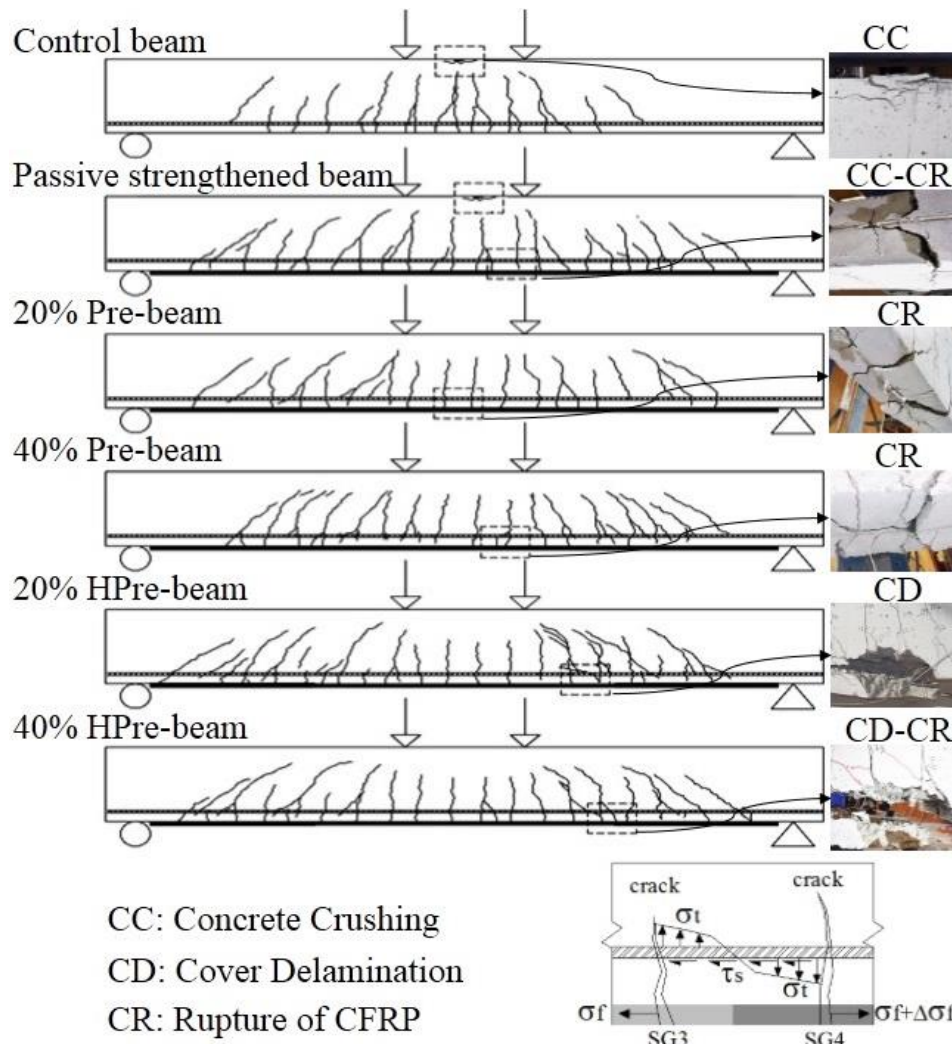Figure 8: Load *versus* concrete compressive strain for strengthened beams

Figure 9: Crack pattern and prevailing failure modes at the ultimate capacity of the tested beams
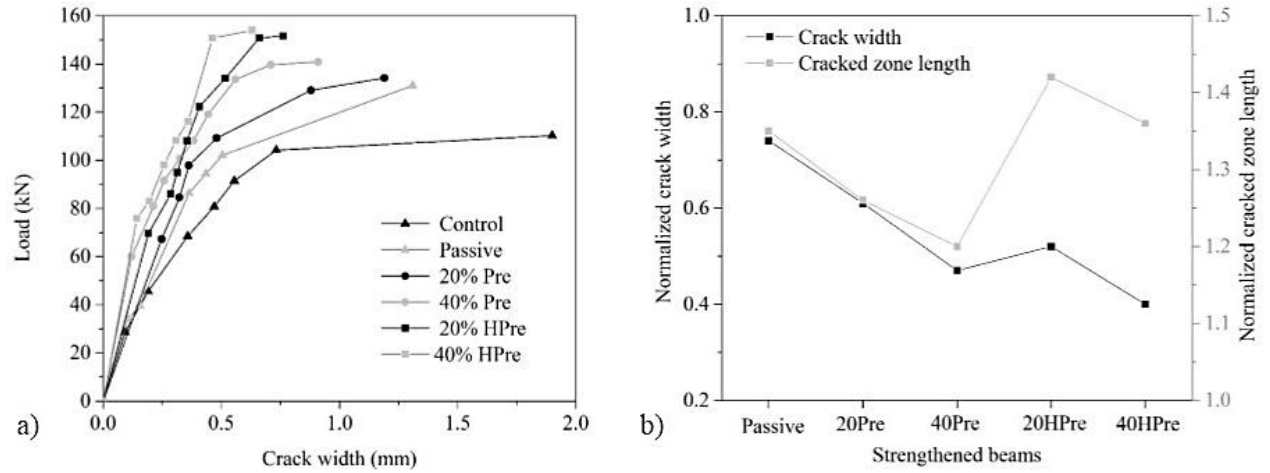
Figure 10: a) Load *versus* crack width of the tested beams, b) cracked zone length and crack width at SLS deflection normalized to the corresponding values of the control beam
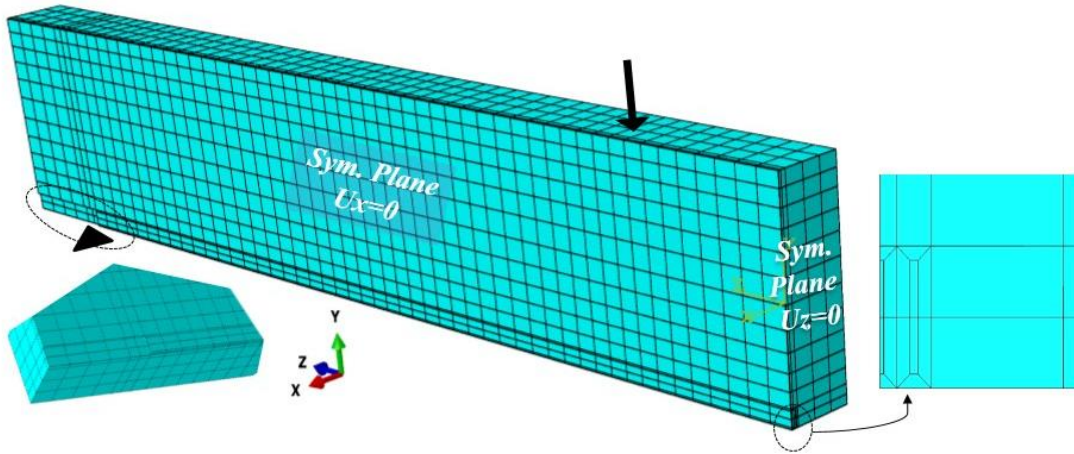
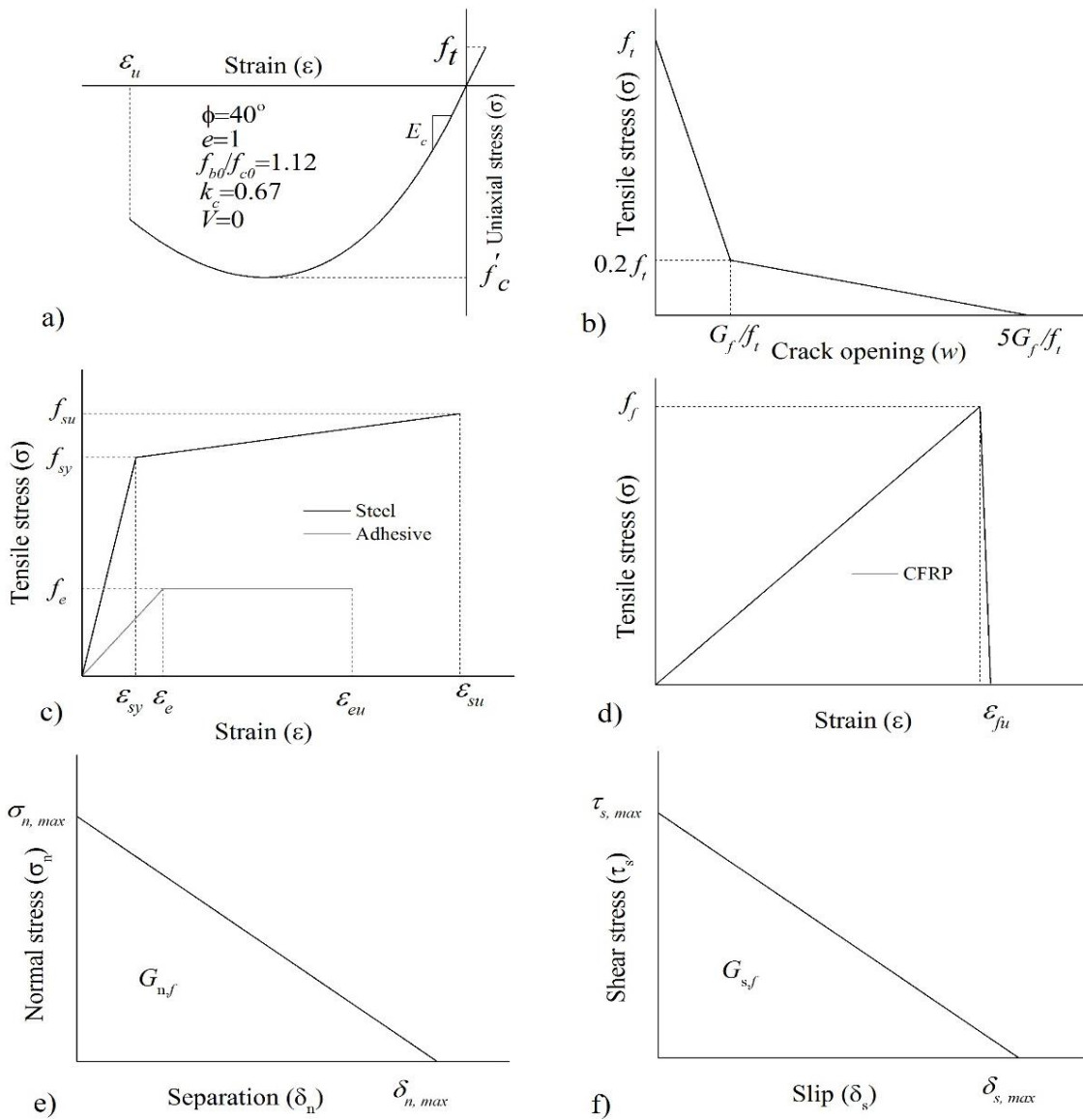Figure 11: Boundary conditions and mesh of the FE model

Figure 12: Uniaxial constitutive laws of the used materials: a) concrete in compression and in tension up to crack initiation, b) concrete post-cracking, c) steel reinforcement and epoxy adhesive, d) CFRP reinforcement, e) normal stress-separation relationship of the interface, f) shear stress-slip relationship of the interface
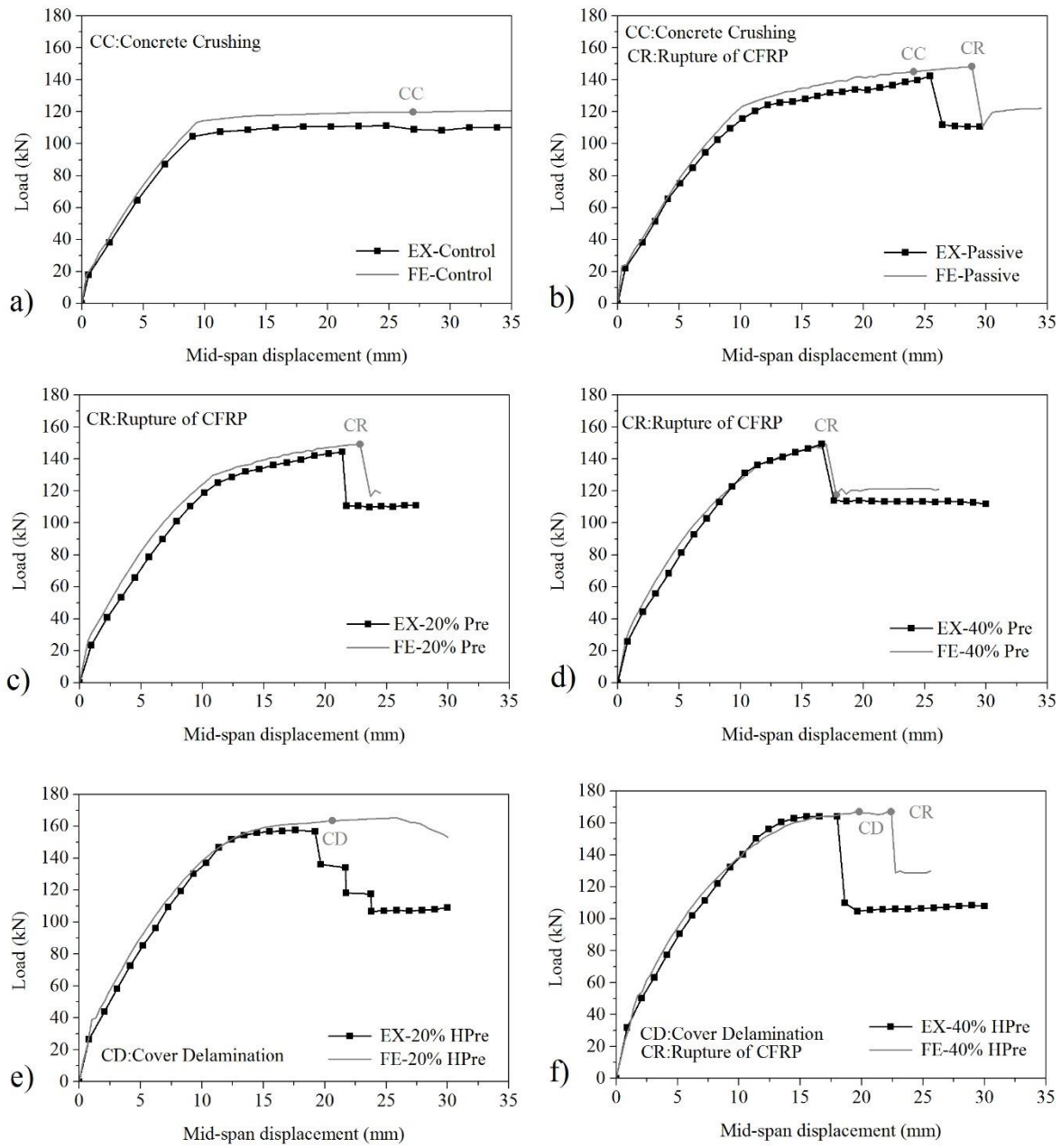
Figure 13: Numerical simulation of the experimental tests: a) control beam, b) passive strengthened beam, c) 20% Pre-beam, d) 40% Pre-beam, e) 20% HPre-beam, f) 40% HPre-beam
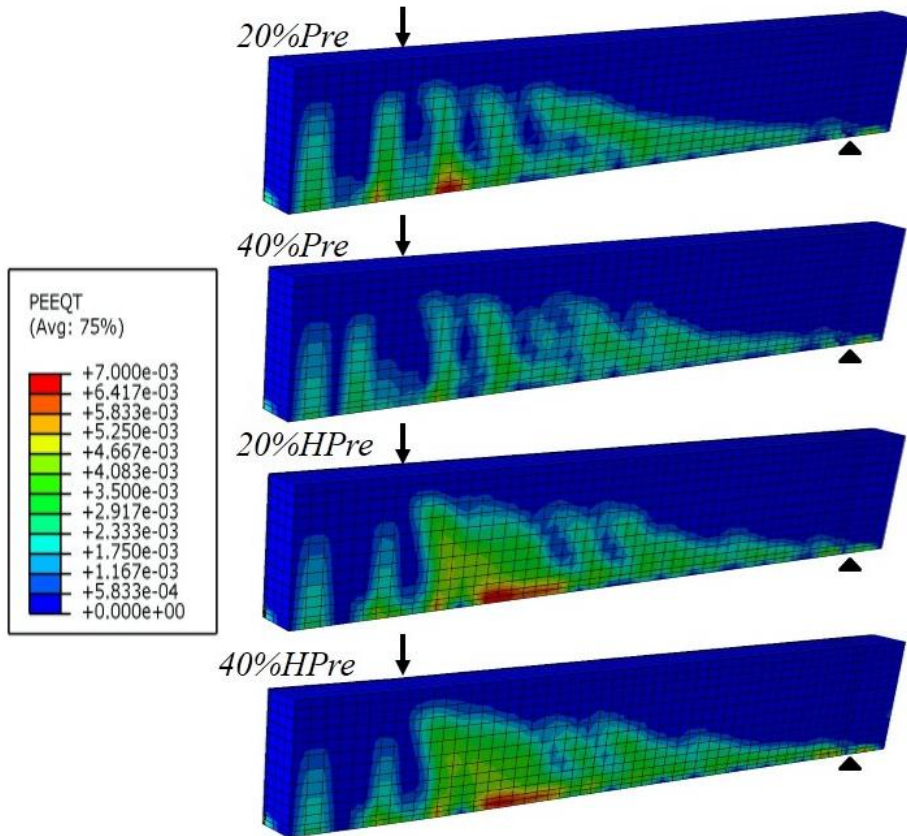
Figure 14: Distribution of the concrete tensile strain based on the PEEQT output
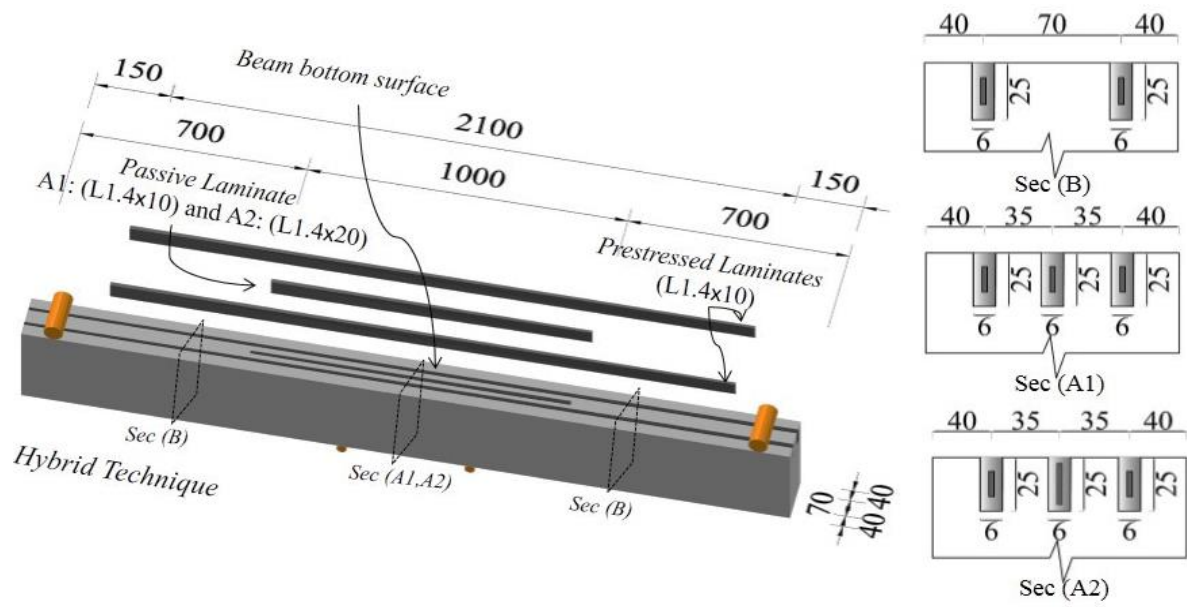
Figure 15: Characteristics of another configuration for the hybrid technique (dimensions in mm) (the beam is intentionally represented upside down to reveal the grooves)
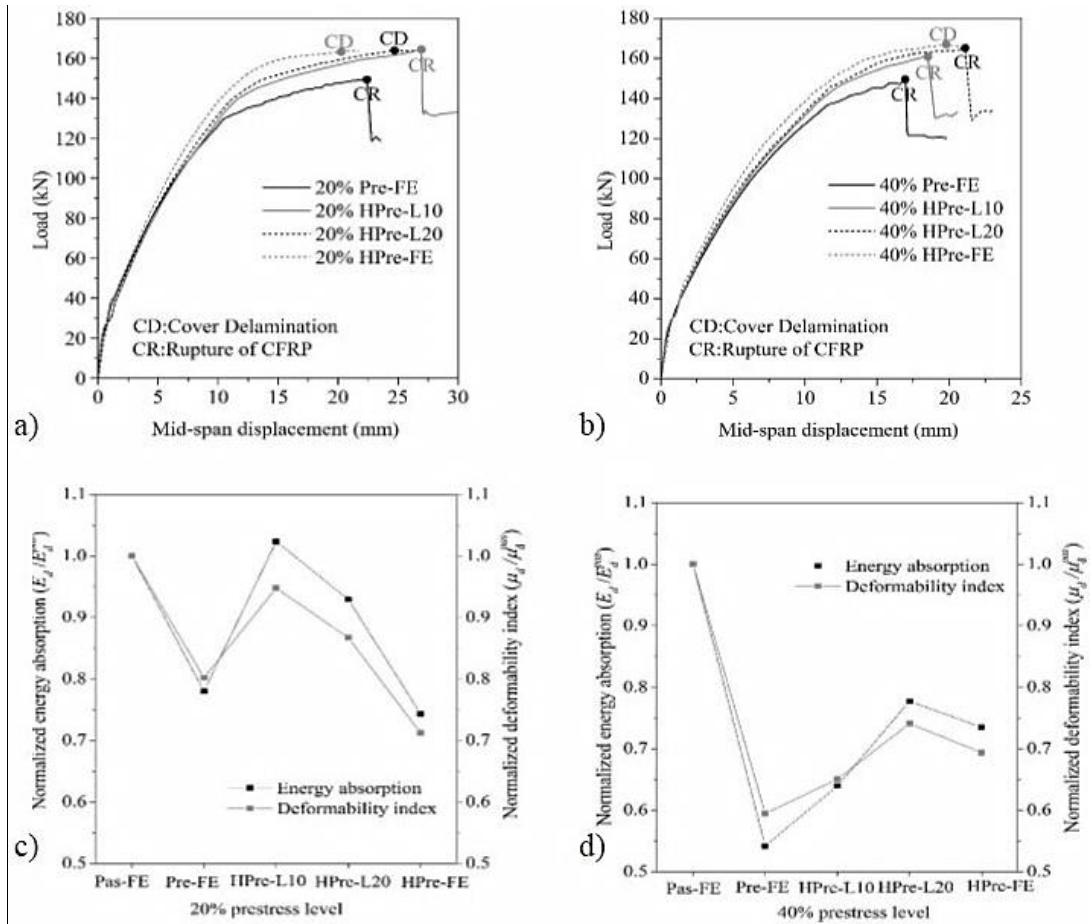
Figure 16: a) load *versus* mid-span displacement of 20% hybrid beams, b) load *versus* mid-span displacement of 40% hybrid beams, c) normalized energy absorption and deformability indexes for 20% prestress level, d) normalized energy absorption and deformability indexes for 40% prestress level

Table 1: The average values of the main material properties of the constituent materials

Concrete	Compressive strength		Young's modulus	
	f_{cm}= 24.5 MPa		E_c=20 GPa	

Steel bars	Diameter	Yield initiation strength	Tensile strength	Elasticity modulus
	6 mm	f_{sym}=613 MPa	f_{sum}= 696 MPa	E_s=218 GPa
	12 mm	f_{sym}=563 MPa	f_{sum}= 656 MPa	E_s=203 GPa

CFRP laminate	Tensile strength	Ultimate tensile strain	Elasticity modulus
	f_{fum}= 1922 MPa	ε_{fum}= 11.7 (‰)	E_f=164 GPa

Epoxy adhesive	Tensile strength	Elasticity modulus
	f_{em}= 20 MPa	E_e=7 GPa

Table 2: Relevant results obtained in the tested beams

RC beams	ρ_f (%)	P_{cr} (kN)	δ_{cr} (mm)	P_y (kN)	δ_y (mm)	P_u (kN)	δ_u (mm)	P_{SLS} (kN)	E_d (kN − mm)	μ_d (δ_u/δ_{SLS})
Control	0	18.00	0.51	104.50	9.01	111.39	24.79	102.68	2284	2.82
Passive	0.065	22.10	0.60	115.84	10.17	142.48	25.43	107.10	2721	2.89
20% Pre	0.065	23.39	0.85	122.18	10.45	144.52	21.40	108.88	2226	2.43
40% Pre	0.065	25.81	0.90	131.17	10.59	149.40	16.60	117.95	1688	1.89
20% HPre	0.195	26.55	0.80	146.83	11.28	156.80	19.20	124.75	2203	2.18
40% HPre	0.195	31.68	0.90	150.31	11.41	164.20	18.00	127.17	2099	2.04

-ρ_f is the CFRP reinforcement ratio at mid-section of the beams;
-P_{cr} is the load at cracking initiation, and δ_{cr} its corresponding deflection;
-P_y is the load at yielding of tensile bars, and δ_y its corresponding deflection;
-P_u is the maximum load, and δ_u its corresponding deflection;
-P_{SLS} is the load at SLS conditions;
-E_d is energy absorption index;
-μ_d is deformability index.

Table 3: Relevant results obtained in the tested beams

RC beams	$\dfrac{P_{SLS} - P_{SLS}^{control}}{P_{SLS}^{control}}$ (%)	$\dfrac{P_y - P_{SLS}^{control}}{P_{SLS}^{control}}$ (%)	$\dfrac{P_u - P_u^{control}}{P_u^{control}}$ (%)	$\dfrac{P_u - P_u^{pas}}{P_u^{pas}}$ (%)	$\dfrac{\delta_u - \delta_u^{control}}{\delta_u^{control}}$ (%)	$\dfrac{\delta_u - \delta_u^{pas}}{\delta_u^{pas}}$ (%)
Control	-	1.77	-	-	-	-
Passive	4.30	12.81	27.91	-	2.58	-
20% Pre	6.04	18.99	29.74	1.43	-13.67	-15.84
40% Pre	14.87	27.74	34.12	4.85	-33.03	-34.72
20% HPre	21.49	42.99	40.76	10.05	-22.54	-24.49
40% HPre	23.85	46.38	47.41	15.24	-27.39	-29.21

- $P_{SLS}^{control}$ is the load of the control beam at SLS conditions;

- $P_u^{control}$ is the maximum load of the control beam, and $\delta_u^{control}$ its corresponding deflection;

- P_u^{pas} is the maximum load of the passive strengthened beam, and δ_u^{pas} its corresponding deflection;

Table 4: Relevant results obtained in the numerical investigation

Prestress level (%)	specimens	$\rho_{f(pas)}$ (%)	$\rho_{f(pre)}$ (%)	P_y (kN)	δ_y (mm)	P_u (kN)	δ_u (mm)	μ_d (δ_u/δ_{SLS})	E_d (kN − mm)
0%	Pas-FE	0.065	-	123.29	10.12	148.17	28.42	3.23	3306.22
20%	Pre-FE	-	0.065	129.64	10.84	149.12	22.82	2.59	2578.87
	HPre-L10	0.032	0.065	139.64	11.61	164.22	26.96	3.06	3383.21
	HPre-L20	0.065	0.065	144.23	12.26	163.75	24.71	2.80	3071.48
	HPre-FE	0.129	0.065	154.41	13.07	163.07	20.25	2.30	2456.89
40%	Pre-FE	-	0.065	136.70	11.57	149.30	16.95	1.92	1790.97
	HPre-L10	0.032	0.065	144.34	11.97	162.02	18.52	2.10	2113.53
	HPre-L20	0.065	0.065	146.99	12.21	165.02	21.10	2.393	2568.86
	HPre-FE	0.129	0.065	159.20	14.16	166.89	19.79	2.24	2428.90

-$\rho_{f(pas)}$ is the passive CFRP reinforcement ratio at mid-section of the beams;
-$\rho_{f(pre)}$ is the prestressed CFRP reinforcement ratio at mid-section of the beams.